RESEARCH ARTICLE

A Deep Neural Network-Based Optimal Power Flow Approach for Identifying Network Congestion and Renewable Energy Generation Curtailment

REHMAN ZAFAR[ID], (Student Member, IEEE), BA HAU VU[ID],
AND IL-YOP CHUNG[ID], (Member, IEEE)
School of Electrical Engineering, Kookmin University, Seongbuk-gu, Seoul 02707, Republic of Korea
Corresponding author: Il-Yop Chung (chung@kookmin.ac.kr)

ABSTRACT Herein, we propose a novel method for identifying power congestion and renewable energy source (RES) power curtailment in power grids by using deep neural network (DNN)-based optimal power flow (OPF) analysis. Synthetic data for load demand and RES power generation are used to obtain the OPF solutions by using an OPF solver. RES locations are selected based on an analysis of the congestion cases, and the DNN is trained by using the load demand and RES power as inputs and the OPF solution as the output. Thereafter, post-processing is performed on the DNN-OPF output by using network information. The final results show the accuracies of identified values on RES curtailment, line loading, generation dispatch schedule, and total generation operating cost. The IEEE 39-bus system was adopted as a case study to validate the proposed model. The results demonstrate that the proposed scheme is much faster and more suitable for transmission systems than conventional OPF methods. Furthermore, the normalized root-mean-squared error was less than 1%, and the computational time was more than 30 times faster than conventional OPF analysis.

INDEX TERMS Deep neural network, network congestion, optimal power flow, power curtailment, renewable energy sources.

I. INTRODUCTION

Nowadays, the integration of renewable energy sources (RESs) in an electric power system is inevitable owing to their environmental and economic benefits [1]. However, the intermittent nature of the RESs can cause various issues for power systems, including transmission-line congestion due to surplus power generation during particular weather conditions. The congestion in the electrical power network can lead to further significant problems, such as power equipment trips, line overloading, outages, and voltage instability [2]. The identification of network congestion is therefore a

The associate editor coordinating the review of this manuscript and approving it for publication was Ruisheng Diao[ID].

fundamental step for achieving reliable and secure power-system operation in the presence of the uncertainty caused by variable RES generation.

Conventionally, to deal with network congestion identification, system operators are required to run an optimal power flow (OPF) analysis. This has become a key tool for many system operators in terms of system planning and real-time operation [3], [4]. OPF analysis is a nonlinear, non-convex, and large-scale optimization problem involving both continuous and discrete variables [5]. The results include the optimal economic dispatch and power flows, which are obtained by considering the system constraints and equipment operating limits [6]. Indeed, system operators need to continually balance a system incorporating RESs [7]. With many constraints

and variables in large-scale systems, the problem becomes more complex and often demands a large amount of computational time to solve [3].

In recent years, dealing with OPF analysis has become more cumbersome because of variable power generation from RESs. Because of abrupt changes that can occur during power generation from RESs widely scattered throughout the power network, prompt network congestion identification and management within a short time period is required. This necessitates the analysis of a large number of scenarios and cases based on frequent and real-time OPF solutions. Regarding large and complex systems, OPF analysis, which itself is a nonlinear and non-convex problem, requires significant running time that can lead to system failure and cascaded blackouts [8]. To deal with this problem, a fast and reliable solution is required. Recently, machine-learning- and deep-learning-based solutions have been mentioned in the literature [9]. These approaches use machine-learning or deep-learning algorithms to predict OPF solutions for given load demands for a particular configuration. These create faster solutions with lower computational burdens that can replace the conventional optimization solvers for OPF analysis. Therefore, these methods are vital for congestion identification and RES curtailment. In this context, we propose a deep neural network (DNN)-based approach for congestion identification and RES power curtailment. A DNN was selected based on its proven significance for engineering problems [10].

Several examples of using a machine-learning approach for OPF analysis mentioned in the literature are typically labeled as learning-based OPF or DNN-OPF analysis. A few examples of these are summarized in Table 1. According to the standard procedure, the machine-learning model is trained on the given input and output of a conventional OPF analysis. In this way, the output data are mapped onto the input data without performing optimization or running OPF analysis software. In [11], a DNN model was used to map the load demand of generators to their bus voltage magnitudes and power dispatch. The authors employed MATPOWER to run the OPF analysis to construct an input and output dataset; the speed and accuracy of the proposed model were faster than an OPF solver with reasonable precision. In [12], a neural network and random forest-based security-constrained OPF (SCOPF) model was proposed. This approch used multi-target regression and considered the input as local information, which it mapped to the output as the power generation was dispatched. Furthermore, the authors created a dataset from a grid optimization (GO) competition including load data, transmission-line data, and contingency scenarios as the input data, while the output comprised generator dispatch power. To obtain this detailed dataset, the authors ran PSS/E on the IEEE-14 bus system and an IEEE RTS 96 test power system.

Similarly, [13] presented various artificial intelligence (AI) algorithms to map OPF solutions. Among them, gradient boosting regression exhibited the best performance with improved computational time and solution accuracy. Load

TABLE 1. Summary of the learning-based opf examples in the literature.

Ref.	AI Algorithm	OPF Tool	Input	Output
[11]	Deep neural network	MATPOWER	Load data	Power dispatch and voltage
[12]	Neural network and a random forest	PSS/E	Load data	Power dispatch
[13]	Gradient boosting regression algorithm	MATPOWER	Load data	Power dispatch
[14]	stochastic gradient boosting tree	N/A	Load data RESs data	Power set points of energy storage
[16]	Random forest	MATPOWER	Load data	Voltages and angles
[17]	Graph neural networks	N/A	Load data	Power dispatch
[18]	Graph neural networks	Pandapower	Load data	Power dispatch
[21]	Deep reinforcement learning	PYPOWER	Load data RES data	Power dispatch and voltage
This study	Deep neural network	MATPOWER	Load data RESs data	Power dispatch, line loading, RESs curtailment and congestion identification

demand was considered as the input, while dispatched real and reactive power along with voltage level were the outputs. The authors also used MATPOWER to perform OPF analysis for the output variables. A case study was also presented using the IEEE-30 bus system, and more than 90% of predictions were within 5% of the true solution. However, approximately 60% of the predictions violated one of the network constraints.

In [14], the stochastic gradient boosting tree (SGBT) algorithm was used to map the optimal solution of nonlinear programming considering community energy storage under uncertainty. The objective of the SGBT learning model was to predict the active and reactive power setpoints of energy storage. The results show 98% optimality for even small data samples.

In another study [15], the authors proposed a DNN approach referred to as DeepOPF to solve the SCOPF problem. They considered load data as the input, while the output provided the real power dispatch of the generators. The authors ran PYPOWER to obtain the OPF solutions and then mapped the input to the output using a DNN-based architecture. The results showed that, compared with a state-of-the-art solver, DeepOPF provided viable solutions with less than
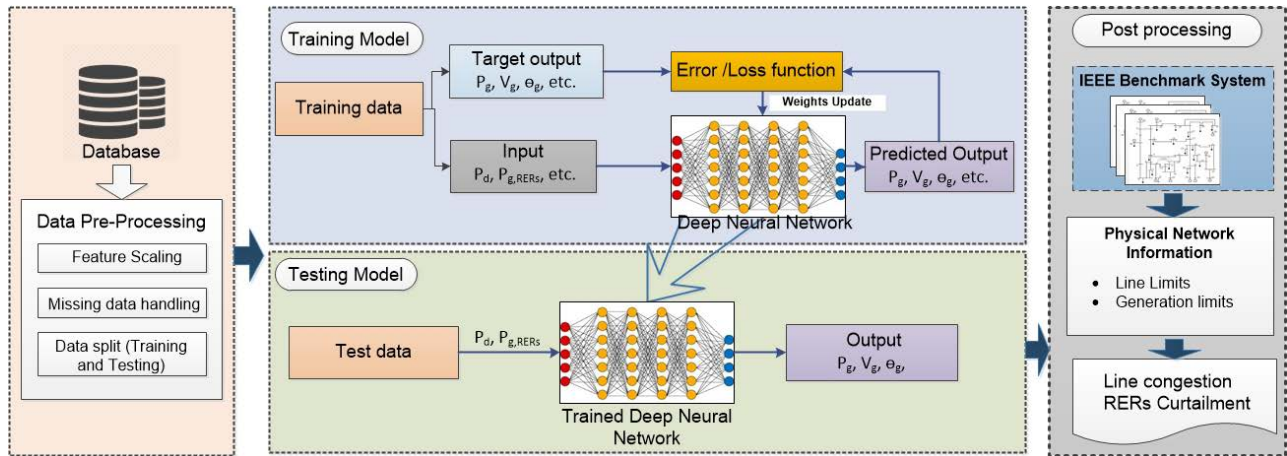
FIGURE 1. Proposed DNN-OPF architecture.

0.2% optimality loss, while reducing the computation time by up to two orders of magnitude. In [16], a multi-input–multi-output (MIMO) random forest model was applied to obtain network voltages and bus angles. Subsequently, network equations were used to calculate the current injection, as well as the real and reactive power injections at various buses. The GO competition repository provided access to a dataset of 500 bus transmission systems, and the OPF analysis was run on MATPOWER to obtain the solution. The load data were considered as input, while the voltage and angle were obtained as the output, both of which were mapped by using a machine-learning-based model. Finally, the power generation plan was calculated by using the output from the machine-learning algorithm. The proposed technique was more computationally efficient than using MATPOWER, and all of the network constraints were satisfied.

A warm-starting OPF with graph neural networks (GNNs) was presented in [17]. Synthetic data were created for two power systems in Illinois and Texas containing 200 and 2,000 buses, respectively. Load data were used as the input data, while the real power scheduling was the output. Similarly, in [18], a GNN-based OPF analysis was presented for an interior-point solution. The authors used the Pandapower software to produce a dataset with the load data being created via a uniform distribution method. They concluded that the proposed method was significantly faster than conventional OPF solvers.

In [19], the authors applied a novel approach to the problem and used the predicted results for further analysis. First, a random forest model was trained to predict the solution of an OPF analysis when given the load demand as input. However, instead of using the predicted results of the model as an OPF solution as is, the results were used as the starting point for the solver. This system exhibited better results than a direct current warm and flat-start.

There are a few studies in which a combination of AI algorithms was used. For instance, in [20], the authors used a neural network and reinforcement-learning techniques to perform OPF. The weights were initialized by imitation learning by the neural network in the deep reinforcement technique to lower the computational burden while training the agents to solve the OPF problem. Similarly in [21], a neural network with reinforcement learning was used to perform real-time OPF to deal with the uncertainties from loads and RESs. In [22], as well as integrating a neural network and reinforcement learning, the authors also included transformer tap changes and distribution grid congestion management in their study.

For further reading on state-of-the-art AI-based OPF, see [23], [24], [25], and [26]. Reference [27] presents a survey related to AI-based OPF. The advantage of AI (machine-learning and deep-learning)-based OPF is that the solutions of non-convex, large systems can be obtained significantly faster than those of conventional OPF solvers. Because of the increasing integration of intermittent RESs, system operators need to adjust the fixed points of the generators more frequently, which is cumbersome when dealing with large power systems. Therefore, AI-based OPF is worth considering for grid operations.

It is worth noting that very few of the systems presented in this literature review use RESs, so it is important to address network congestion and RES power curtailment accordingly. Herein, we present a DNN-based solution to identify the congestion and determine curtailment of RES power.

The proposed model is applicable at the transmission system operator and distribution system operator levels to identify congestion in a network and anticipate the potential curtailment of RESs. Furthermore, the proposed scheme enables system operators to avoid grid instability during blackouts. The contributions of this paper are summarized as follows:

- A DNN-OPF approach is proposed for large-scale power grids in the presence of RESs.
- A post-processing mechanism for OPF analysis is defined to obtain network congestion identification, RES power curtailment values, line loadings, and generation costs.

The remainder of the paper is organized as follows. The proposed DNN-OPF scheme is detailed in Section II. Section III is dedicated to its implementation details along with a case study. The results are discussed in Section IV. Finally, conclusions are drawn in Section V.

II. THE PROPOSED SCHEME

Here, we propose the DNN-OPF methodology used to deal with the identification of congestion and the quantification of power curtailment in the presence of RESs.

Fig. 1 shows the architecture of the proposed scheme. A database obtained from a conventional OPF tool such as MATPOWER can be used in this framework. In practice, historical operation data can be taken from the database of the system operator's energy management system. Next, the data are moved to the pre-processing phase where tasks such as missing data handling, feature scaling, and data division are performed. The dataset is divided into training data, validation data, and testing data.

The model is then trained using the training data via mapping of the inputs and outputs. In the training phase, the data are divided into targeted and input values. Following the standard training procedure, the input data are sent to the DNN, and the results are compared with the targeted values by using the error/loss function.

In the testing phase, the input data are fed to the trained network, and the output is obtained. The acquired outputs are used in the post-processing phase during which further desired parameters related to the transmission network are calculated.

A. DATABASE CREATION AND PRE PROCESSING

Fig. 2 shows the procedure for dataset creation. The data move to the pre-processing phase during which missing data handling, feature scaling, and data division tasks are performed. The data created are split into training and testing datasets. In this study, the OPF analysis is performed using synthetic data with N samples for power demand P_d and power generation from the RESs (i.e., $P_{g,RESs}$) taken as an input. The data on the power demand and generation from RESs are created by considering uniformly distributed random numbers in certain ranges of data given by the IEEE benchmark system. We used the IEEE 39-bus system to obtain the OPF analysis results.

We used MATPOWER 7.1 [28] in the MATLAB 2021a environment to run the OPF. In this study, MATPOWER Interior Point Solver (MIPS) is used to solve the OPF problem. MIPS can be used to solve nonlinear programming problems (NLPs) via the primal-dual interior-point method. The load demand and RES power generation are used as input, and the output is obtained in terms of the generation dispatch for all of the other parameters related to the OPF, such as the associated voltages and angles. However, for real systems, this input and output can be replaced by using historical datasets for the particular transmission system.
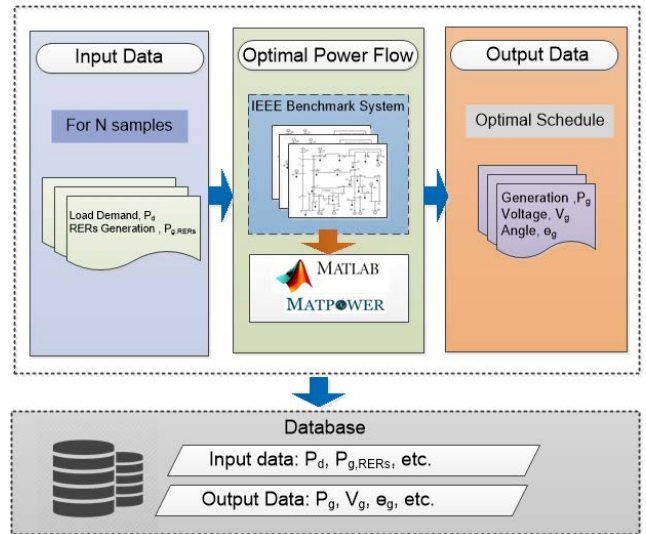

FIGURE 2. Database creation procedure.

Conventionally, the modeling for OPF analysis is described by using (1)–(9). Equation (1) presents the objective function aimed at minimizing the overall operating cost that is subject to the power flow and generation constraints for $i = 1 \ldots n_g$ generators and $j = 1 \ldots n_b$ buses.

1) OBJECTIVE FUNCTION

$$\min f(P_g) = \sum_{i=1}^{n_g} C_p^i(P_g^i), \tag{1}$$

where C_p^i is the polynomial cost function of the active power (P_g^i) of the generators. These are subject to the following constraints.

Equations (2) and (3) present the power equality constraints for active and reactive power generation and consumption in the network, respectively.

2) POWER EQUALITY CONSTRAINTS

$$(P_g^j - P_d^j) - Re\left\{ V_j \left(\sum_{k=1}^{n_b} Y_{jk} V_k \right)^* \right\} = 0, j = 1 \ldots n_b, \tag{2}$$

$$(Q_g^j - Q_d^j) - Im\left\{ V_j \left(\sum_{k=1}^{n_b} Y_{jk} V_k \right)^* \right\} = 0, j = 1 \ldots n_b, \tag{3}$$

where P_g^j and Q_g^j are the generated active and reactive power and P_d^j and Q_d^j are the active and reactive load power at bus j, respectively. V_j the voltage at bus j, Y_{jk} is the admittance between bus j and k and V_k is the voltage at bus k.

Equations (4) and (5) are the constraints related to line flow from and to the bus, respectively.

3) MAXIMUM LINE CAPACITY CONSTRAINTS

$$\left|F_f(\theta, V)\right| - F_{\max} \leq 0, \qquad (4)$$

$$\left|F_t(\theta, V)\right| - F_{\max} \leq 0, \qquad (5)$$

where F_f and F_t are the line flows from and to the bus, respectively, and $F_{\max}$ is the maximum capacity of the line.

4) BUS VOLTAGE AND ANGLE LIMIT CONSTRAINTS

$$\theta_j^{\min} \leq \theta_j \leq \theta_j^{\max}, j = 1 \ldots n_b, \qquad (6)$$

$$V_j^{\min} \leq V_j \leq V_j^{\max}, j = 1 \ldots n_b, \qquad (7)$$

where $\theta_j^{\min}$ and $\theta_j^{\max}$ are the minimum and maximum voltage angle limits, and $V_j^{\min}$ and $V_j^{\max}$ are the minimum and maximum voltage limits at bus j, respectively.

5) GENERATION LIMIT CONSTRAINTS

$$P_g^{i,\min} \leq P_g^i \leq P_g^{i,\max}, i = 1 \ldots n_g, \qquad (8)$$

$$Q_g^{i,\min} \leq Q_g^i \leq Q_g^{i,\max}, i = 1 \ldots n_g, \qquad (9)$$

where $P_g^{i,\min}$ and $Q_g^{i,\min}$ are the minimum active and reactive generation limits, and $P_g^{i,\max}$ and $Q_g^{i,\max}$ are the maximum active and reactive generation limits of the *ith* generator, respectively.

6) FUEL COST CURVE

Generator curves are commonly expressed as cubic or quadratic functions or as piecewise linear functions. In this study, we applied a quadratic fuel cost function as follows:

$$C_p^i(P_p^i) = \alpha + \beta(P_p^i) + \gamma(P_p^i)^2, \qquad (10)$$

where C_p^i is the operating cost; P_g^i is the output power; and α, β, and γ are the cost coefficients of the *ith* generator.

B. THE TRAINING PHASE

In the training phase, the data are divided into target values and input values.

The input data (e.g., the demand (P_d) and RES generation ($P_{g,RESs}$)) are sent to the DNN, and the results are obtained and compared with the targeted values (generation dispatch ($P_{g,disp.}$), injected RES power ($P_{inj,RESs}$), voltage information (V_g), etc.) by using the error/loss function.

The hyperparameters are tuned by considering error/loss minimization. The tuning procedure for the DNN is detailed in the implementation section.

C. THE TESTING PHASE

In the testing phase, the input data such as P_d and $P_{g,RESs}$ are inputted into the trained network, after which the output is obtained and the error is measured by using performance parameters. If the error is within the desired range, the training is considered to be complete and ready to use as a replacement for conventional OPF.

The performance parameters used in this study are the root mean square error (RMSE) (11), normalized RMSE (NRMSE) (12), mean absolute error (MAE) (13), and normalized MAE (NMAE) (14) (RMSE and MAE are normalized based on the mean values):

$$RMSE = \sqrt{\frac{1}{N} \sum_{i=1}^{N} \left(x_i^a - x_i^p\right)^2}, \qquad (11)$$

$$NRMSE = \frac{RMSE}{\overline{x^a}} * 100\%, \qquad (12)$$

$$MAE = \frac{1}{N} \sum_{i=1}^{N} \left|x_i^a - x_i^p\right|, \qquad (13)$$

$$NMAE = \frac{MAE}{\overline{x^a}} * 100\%, \qquad (14)$$

where x_i^a and x_i^p are the actual and predicted points, respectively, $\overline{x^a}$ is the average of the actual values, and N is the total number of samples.

D. THE POST-PROCESSING PHASE

The output data obtained from the trained DNN-OPF and the physical network information are used in the post-processing phase for network congestion identification, RES power curtailment, and network line-loading conditions updated generator dispatch schedule, RES power injection, and total generation cost. The post-processing phase has the following four steps.

Step 1: The power dispatch schedule generated by the DNN model is evaluated for constraint violations. First, it is checked to see whether it violates the minimum and maximum generating limits. If the generation points are violated, the points are set within the generation limits by using (15) and (16):

$$P_{g,disp.}^i = P_g^{i,\min}, \text{ if } P_{g,disp.}^i \leq P_g^{i,\min} \text{ for } i = 1 \ldots n_g, \qquad (15)$$

$$P_{g,disp.}^i = P_g^{i,\max}, \text{ if } P_{g,disp.}^i \geq P_g^{i,\max} \text{ for } i = 1 \ldots n_g, \qquad (16)$$

where $P_{g,disp.}^i$, $P_g^{i,\max}$, and $P_g^{i,\min}$ are the real power-generation dispatch, and the minimum and maximum levels of the generation power of the *ith* generator.

Next, the power balance is maintained if the output generation plan violates the load balance. If the total generation is less than the load demand, the power of RES is first increased by considering a reduction in curtailment (this operation is performed if the line is not predicted as congested). Subsequently, other generators are considered to have input power based on cost prioritization (from the lowest generation cost to the highest) until generation balance is achieved.

Similarly, if the total generation exceeds the demand, the power starts to drop from the most costly generation to the cheapest one until the power balance is maintained. The power generations are kept within the limits while balancing the load.

Step 2: Based on the DNN-OPF model, the power injected from the RESs is observed at the RES generator bus. If the

injected power from the RESs ($P_{inj,RESs}$) at the output of the OPF analysis is less than the available RES power ($P_{g,RESs}$) at the input, the output of the corresponding RESs was curtailed to meet the system constraints and avoid network congestion in the line. The amount of RES power curtailment at the associated bus can be calculated as

$$P_{curtailed,RESs} = P_{g,RESs} - P_{inj,RESs}, \quad (17)$$

where $P_{curtailed,RESs}$ is the curtailed power value, $P_{g,RESs}$ is the injected power, and $P_{g,RESs}$ is the available RES power.

Step 3: Network congestion is identified via RESs curtailment scenarios and line loading information. If there is curtailment on the RES bus, then the line is considered congested. Otherwise, congestion is also verified by analyzing the line loadings of the network.

Step 4: Finally, the cost of the generation dispatch is calculated for the updated power-generation combination for each sample by applying (10) according to the power dispatched by each generator.

In summary, post-processing by the DNN-OPF provides the network congestion scenarios caused by excessive RES generation, the expected amount of RES power curtailment, line loadings, updated generator dispatch schedule, RES power injection, and total generation cost.

III. IMPLEMENTATION DETAILS

Here, we discuss the implementation of the proposed DNN-OPF on the IEEE 39-bus system. In the case study, we have analyzed the network for RES location and then created a database for the test power system. The OPF problem is solved by assigning the RESs to different locations. The line-limit capacities are observed for various samples generated from the RESs, and the locations of the RESs are set in such a way as to yield a large number of congestion cases. Thereby, we have created a dataset for DNN-OPF containing the largest possible number of cases. Details of the analysis are discussed in the subsequent subsections.

A. A CASE STUDY

The IEEE 39-bus system is a 10-machine New England power grid [29]. The IEEE-39 bus system is a 345-kV transmission system with 10 generators that can generate a maximum of 7,367 MW. It has 21 loads connected to the system with a peak of 6,254 MW.

In the network, buses are connected to 46 branches including six tie lines that connect three areas, as illustrated using three different colors in Fig. 3. The network and cost data used in the study were obtained from [30]. Table 2 presents detailed information on the IEEE 39-bus system. The cost coefficients of generators 'α' and 'γ' were set to zero in the provided case data file, whereas 'β' was given a range of 6.72 to 34.84 \$/kWh.

B. SELECTION OF THE RES LOCATIONS

Because of the limited capacity of transmission lines and the minimum generation limits of conventional generators, the
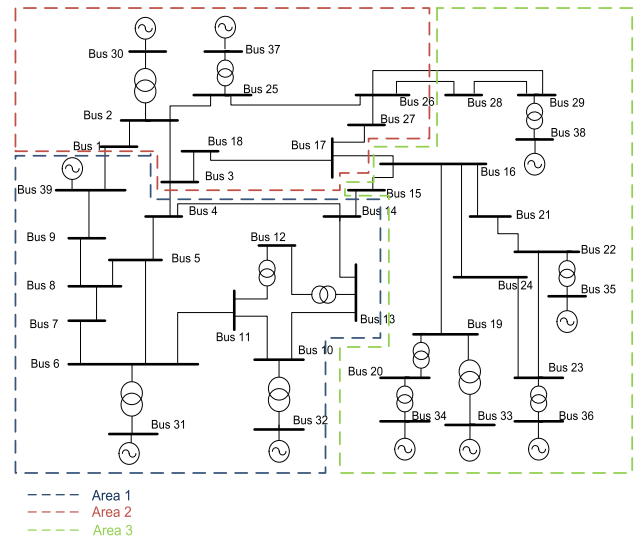

FIGURE 3. IEEE 39-bus system.

TABLE 2. Summary of the IEEE 39-bus system.

Items	Quantity
Generators	10
Loads	21
Branches	46
Tie lines	6
Areas	3

distribution of RESs is directly related to network congestion problems. Accordingly, the distribution of RESs in a power system greatly affects the long-term development plan for the system, such as designs for new transmission lines and tie lines, the integration of new generation technologies, and the enhancement of system flexibility.

To analyze the impact of RES distribution, OPF analysis is performed by considering different RES locations and different levels of load demand and RES output power. In this study, three buses (5, 16, and 18) are selected as RES locations because each of them is particularly important for network congestion problems in one of the three areas. Bus 18 has the lowest thermal limit among the connected branches in area 2 whereas bus 16 has the highest limit among the connected branches in area 3. Bus 5 is selected in area 1 to represent the medium-range capacity limits for connected branches.

Two scenarios are considered and compared. In scenario 1, a RES plant is installed at one location while in scenario 2, two RES plants are installed at two locations among buses 5, 16, and 18. In each scenario, total RES-rated power of 2,000 MW is considered.

To evaluate the impact of network congestion due to RES integration, 10,000 operation cases with various RES generation power levels and different loading conditions are performed. The load demand varied from 60% to 100% of the system's peak load. In addition, at each load level, the total maximum RES power varies from 100 to 2,000 MW.

For the OPF calculation, we input the generation costs of all of the generators while the generation cost of the RES is set to zero. After solving the OPF problem, if the scheduled power of RES is less than its available power, we are able to identify the amount of RES power curtailment required to meet the network constraints. In each scenario, the number of congestion cases is counted to make further comparisons.

Fig. 4 presents the percentage of congestion cases in scenario 1. The results indicates that the percentage of cases depended on the RES location and output power level. Among the three considered locations for the RES, the case with a single RES plant installed at bus 16 has the lowest percentage of congestion. In contrast, the case with a single RES plant installed at bus 18 results in the highest percentage of congestion. This is due to the limited branch capacity of connections with bus 18. As shown in Fig. 3, there are only two transmission lines connected with bus 18 (from bus 3 to bus 18 and bus 17 to bus 18) with a total transmission capacity of 1,100 MW. In contrast, five transmission lines are connected to bus 16.
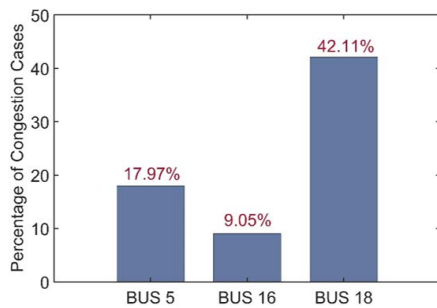

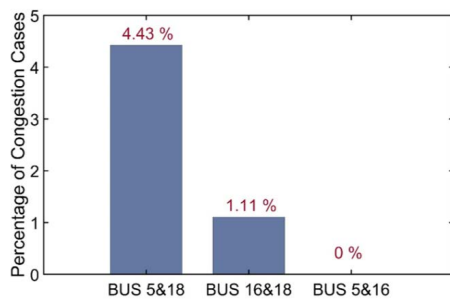**FIGURE 4.** Percentage of congestion cases in scenario 1 (RES at one location).

FIGURE 5. Percentage of congestion cases in scenario 2 (two RESs at two locations).

Fig. 5 presents the percentage of congestion cases for scenario 2. To create the dataset, we select the RES locations as buses 5 and 18 because we require additional congestion cases to train the network for such scenarios.

C. PDATABASE FORMATION
We create a dataset for DNN-OPF after considering the analysis of the impact of the RES distribution. To create the dataset,

the RES locations are set as buses 5 and 18. Overall, we have created 10,000 samples for both the RESs and the load. For the RESs, we have generated a random sample from 10% to 130% of 1,500 MW, yielding a maximum of approximately 2,000 MW (this is related to the analysis conducted in the previous section). While considering the provided demand as the peak load, we vary the load from 10% to 100% by using the given data in the PGlib benchmark for the IEEE 39-bus system [30].

After generating the input data, the OPF analysis has run using MATPOWER to obtain the output for 10,000 input samples. Based on the OPF output, we have selected real power and line loadings as the targeted output for the DNN-OPF analysis.

The dataset formation is shown in Fig. 6 in terms of input and output arrays. For the input, 10,000 samples of a 1×2 array are used for the RESs at two locations (buses 5 and 18). For the output data, we have the same number of samples with a power-generation schedule in the form of a 1×12 array (including two RESs injecting power to the network along with 10 other conventional generators) and a 1×46 array for the line-loading information.
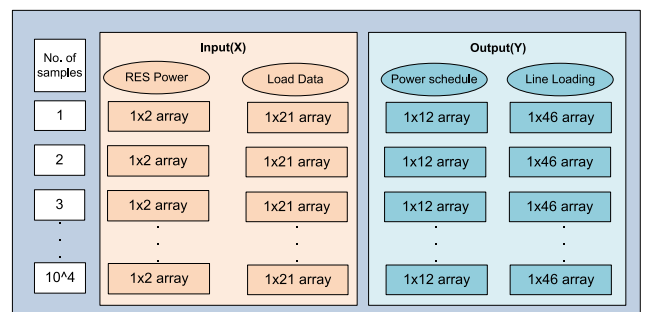

FIGURE 6. Database representation for DNN-OPF.

More output columns can be added according to specific requirements for voltage, angle, and/or any other information based on conventional OPF. For the DNN-OPF analysis, we have used time-series data for a particular site to form the input and output as we are able to forecast the RES and load data by considering the historical data of the real network and location.

The dataset are split into training, validation, and test sets (70%, 15%, and 15% of the overall set, respectively), as reported in Table 3. The validation set is used to tune the parameters for the network and to avoid overfitting or underfitting.

D. HYPERPARAMETER TUNING FOR THE DNN
As previously discussed, hyperparameter tuning is essential when training a DNN. To train the network, hyperparameters for the DNN are tuned by using a search space (Table 4). The tuned network has three hidden layers (rendering it a deep network), as well as input and output layers. The network also has 23 inputs and 58 outputs, making it a MIMO model.

TABLE 3. Dataset division.

Number of Samples		
Training Set	**Validation Set**	**Test Set**
7,000	15,00	15,00

To deal with the backpropagation, the Levenberg–Marquardt (LM) [31], gradient descent (GD) [32], and gradient descent with momentum (GDM) [33] algorithms has been tested. The LM algorithm exhibited the best overall performance with 1,000 epochs and standard feature scaling. Full-batch training was then performed.

TABLE 4. Hyperparameters for the DNN.

Hyperparameter	Tuned Value	Search Space
Hidden Layers	3	2, 3 ,4 ,5
Hidden Units	10	5,10,15,20
Algorithm	LM	LM,GD,GDM
Epochs	1000	500,1000,1500,2000

E. POST-PROCESSING

The output of the DNN-OPF analysis include the line loading and the power-generation dispatch. We next have performed post-processing on the output. First, we have separated the power dispatch for the conventional generators, the RES injected power, and line loading from the output data. Next, line congestion and curtailment values are calculated from the separated data while considering the generation limits and load balance.

The amount of RES curtailment for each dataset sample are calculated by using (17) for the buses containing the RESs. Congestion are detected via the line-loading conditions anticipated from the DNN-OPF analysis and the buses with curtailed RES power.

Furthermore, the generation cost for each sample is calculated by using (10). The RES generation cost is set to zero while other conventional generators has quadratic fuel cost curves. Finally, the accuracies of the RES curtailment, line loading, generation dispatch, and total generation operating cost values are calculated by comparing the results with the conventional OPF analysis results.

IV. RESULTS AND DISCUSSION

Here, the results of the proposed scheme are presented and discussed. The simulations were performed on a desktop computer using Windows 10 with an Intel i7 processor and 16 GB of RAM.

A. THE DNN-OPF TRAINING PERFORMANCE

In this study, We focus on a multivariate regression problem with multiple outputs. Table 5 summarizes the performance evaluation for the proposed DNN-OPF system. The test set and validation set errors are approximately the same. Therefore, we can conclude that no overfitting or underfitting issues

occurred in the trained network. The NRMSE and NMAE results also reveal an overall error of less than 1%.

TABLE 5. Performance evaluation of DNN-OPF.

Performance Matrix	Validation Set	Test Set	Whole Dataset
RMSE (MW)	14.59	14.40	14.11
NRMSE (%)	0.186	0.182	0.177
MAE (MW)	42.77	41.29	42.21
NMAE (%)	0.00938	0.00898	0.00914

Fig. 7 shows a scatter plot for the test set, which reveals the accuracy of the DNN model as the predicted and measured instances were linearly aligned. Fig. 8 shows a comparison of the error between the validation set, the test set, and the entire dataset.
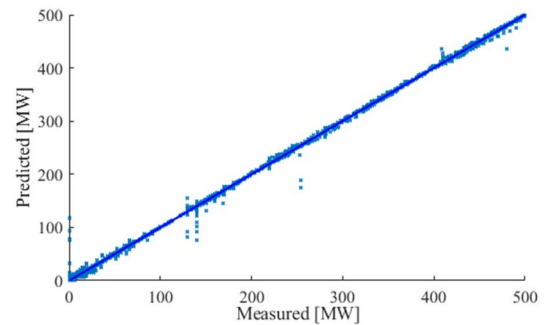

FIGURE 7. Scatter plot of the performance results for the DNN-OPF with the test dataset.
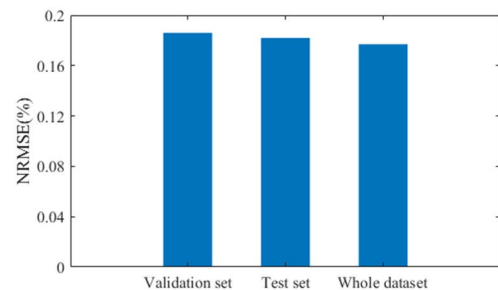

FIGURE 8. Error evaluation of the DNN-OPF.

In addition, we propose post-processing on the predicted instances to acquire congestion information and RES power curtailment values along with power dispatch and total generation cost. The results for post-processing are discussed in the subsequent subsection.

B. POST-PROCESSING RESULTS

In post-processing, we have obtained the RES curtailment, network congestion identification, generator power dispatch scheduling, and total generation cost values. Next, we have calculated the accuracy of the output results, including the curtailment and the generation cost values along with the line

loading of 46 branches and power scheduling of 12 generators. We have used the entire dataset (RES power and load demand) as input to the trained network and obtained the results for the proposed scheme. Subsequently, results are compared with the standard OPF analysis and determined the accuracy in terms of RMSE and NRMSE. Table 6 summarizes the results for the accuracy of the proposed model, while Figs. 9–11 show curve-fitted graphs for the generation dispatch, line loading, and curtailment values.

TABLE 6. DNN-OPF post-processing output accuracy.

| Output Field	RMSE	NRMSE
RES curtailment	3.761 MW	0.0105%
Line loading	6.272%	0.2450%
Generation scheduling	12.368 MW	0.0431%
Total generation cost	$ 519.82	0.0166%
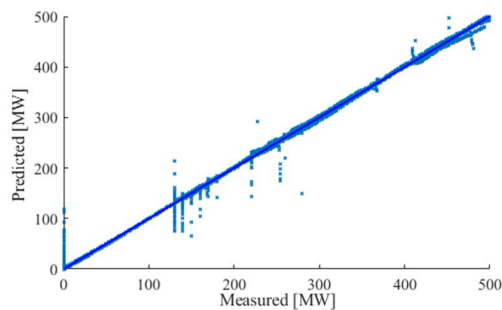
FIGURE 9. Scatter plot of the generation scheduling values.
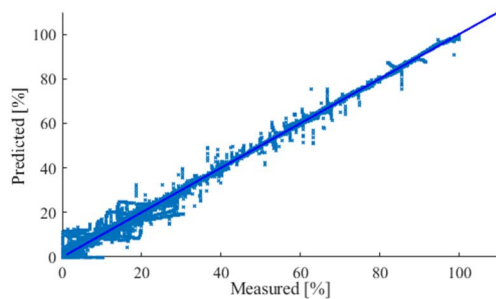
FIGURE 10. Scatter plot of the line loading values.

The results show that the error in the output accuracy using the proposed model is less than 1%, thereby indicating its suitability for many power-system applications that tend to have a margin for error of approximately 1%. Using a DNN-based solution to solve the curtailment and congestion problem in real-time proves to be vital, as it is able to solve the problem quickly. This is particularly beneficial for large networks in which conventional OPF takes a long time to run, especially since the OPF problem can be highly complex and/or non-convex. The proposed solution can also be implemented for the unit-commitment problem, for which many constraints exist. Overall, a DNN can learn complex
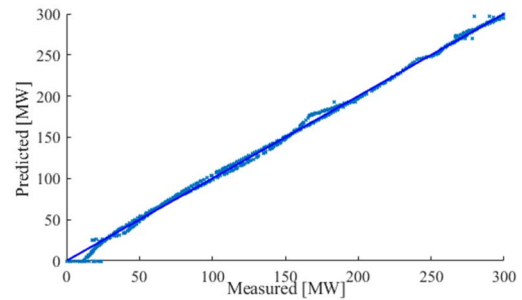
**FIGURE 11.** Scatter plot of the RES curtailment values.

TABLE 7. Computational time comparison.

No. of Samples	OPF Running Time (s)	DNN-OPF Running Time (s)	DNN-OPF Accuracy [NRMSE (%)]
2.5k	36.33	1.015	0.3908
5k	68.78	2.030	0.3881
7.5k	99.99	3.045	0.2271
10k	132.07	4.060	0.1771

equations and perform the required tasks in a fast and efficient manner.

C. RUN-TIME EVALUATION

The proposed method is significantly faster computationally than conventional OPF. For example, the proposed DNN-OPF approach requires 4.06 s for running 10,000 instances of OPF. This means that the DNN-OPF analysis takes 0.406 ms for 1 instance, making it 30 times faster than conventional OPF that takes 132 s to solve the same 10,000 instances. A comparison of the computational times for 2,500, 5,000, 7,500, and 10,000 instances with the associated accuracies are provided in Table 7, while Fig. 12 shows a graphical comparison of the computational times.
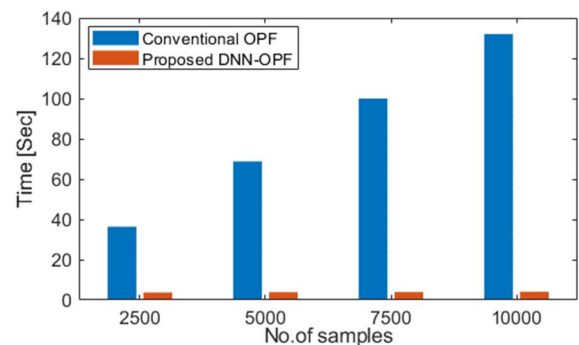
FIGURE 12. Computational time comparison.

D. PERFORMANCE EVALUATION WITH THE NEW DATASETS

The proposed method is evaluated on various datasets to assess its performance in unforeseen operating conditions. A previously trained network on a prior dataset is used for

this purpose. Datasets of 10,000 samples have been generated by using Latin hypercube sampling (LHS) [34], a normal distribution [35], and a Weibull distribution [36] for a range of 10% to 100% of the base case-load values. LHS generates values that are randomly distributed and permuted; the mean and standard deviation for the normal distribution are set to 0.5 and 2, respectively; and the scale and shape factors for the Weibull distribution are set to 10 and 1, respectively. All of the datasets are created by using the MATLAB statistics and machine learning toolbox software [37].

For each dataset, conventional OPF solutions and their accuracies are abtained by using the previously trained network. The results for the new datasets are given in Table 8. Similarly, post-processing accuracies for each dataset are provided in Table 9. Notably, the NRMSEs for each dataset remained under 1%.

TABLE 8. Performance evaluation of the DNN-OPF using the new datasets.

Performance Matrix	LHS	Normal Distribution	Weibull Distribution
RMSE (MW)	17.92	20.32	70.4
NRMSE (%)	0.225	0.255	0.896
MAE (MW)	49.84	50.0824	124.981
NMAE (%)	0.01079	0.01084	0.0274

TABLE 9. DNN-OPF post-processing output accuracy using the new datasets.

Dataset Distribution	Output Field	RMSE	NRMSE
	RES curtailment	5.89 MW	0.0165%
	Line loading	6.61%	0.2583%
LHS	Generation scheduling	12.40MW	0.0572%
	Total generation cost	$548.17	0.0175%
	RES Curtailment	8.14 MW	0.0228%
	Line loading	6.72%	0.2643%
Normal distribution	Generation scheduling	18.65 MW	0.0651%
	Total generation cost	$541.29	0.0173%
	RES curtailment	25.12 MW	0.0694%
	Line loading	13.384%	0.5263%
Weibull distribution	Generation scheduling	68.74 MW	0.2433%
	Total generation cost	$788.03	0.0257%

Hence, the proposed DNN-OPF-based algorithm can provide power-system scheduling, network congestion identification, RES curtailment evaluation, and so on, while having a faster computation time than conventional OPF.

The proposed DNN-OPF-based solution has some prediction errors that occur normally because of stochastic behavior during the training process and the randomness of the datasets. These errors can be minimized by precise training with more datasets and/or advanced post-processing algorithms. In addition, we think that more sophisticated training

algorithms with active constraints according to the system conditions can also be helpful toward improving on prediction errors. Thus, a comprehensive study of the constraints along with error analysis is needed.

Furthermore, the proposed approach has a limitation in that it only works for defined topologies. If the topology changes or N-1 contingencies are considered, the network needs to be retrained to achieve accurate performance. In future work, the proposed model will be enhanced to cope with topological changes and contingency events in addition to error analysis.

V. CONCLUSION

In this study, a DNN-OPF model was proposed to provide fast and reliable OPF solutions that can efficiently predict network congestion and apply RES power curtailment. The results demonstrate that the accuracy of the output from the proposed DNN-OPF model had an error level of less than 1%. Using a DNN-based solution to solve actual RES power curtailment and congestion problems in real-time is vital as such systems can solve them quickly. In particular, the proposed system performed 30 times faster than conventional OPF. Consequently, it is advantageous for optimizing large-scale networks in which traditional OPF solvers take a long period of time to obtain solutions. DNNs are capable of learning complex equations and performing tasks quickly and effectively. Therefore, the proposed method is adaptable to larger-scale problems such as the unit-commitment problem involving multiple constraints that can be complex and/or non-convex.

In future work, error analysis will be performed on the proposed approach and a hybrid approach will be developed to deal with contingencies and topology changes. Accordingly, operating reserves and other market solutions could be used to deal with such issues.

REFERENCES

[1] A. Zahedi, "A review of drivers, benefits, and challenges in integrating renewable energy sources into electricity grid," *Renew. Sustain. Energy Rev.*, vol. 15, no. 9, pp. 4775–4779, 2011, doi: 10.1016/j.rser.2011.07.074.

[2] A. Baczyńska and W. Niewiadomski, "Power flow tracing for active congestion management in modern power systems," *Energies*, vol. 13, no. 18, p. 4860, Sep. 2020, doi: 10.3390/en13184860.

[3] F. Capitanescu, J. L. M. Ramos, P. Panciatici, D. Kirschen, A. M. Marcolini, P. Platbrood, and L. Wehenkel, "State-of-the-art, challenges, and future trends in security constrained optimal power flow," *Electr. Power Syst. Res.*, vol. 81, no. 8, pp. 1731–1741, Aug. 2011, doi: 10.1016/j.epsr.2011.04.003.

[4] S. S. Reddy and P. R. Bijwe, "Multi-objective optimal power flow using efficient evolutionary algorithm," *Int. J. Emerg. Electr. Power Syst.*, vol. 18, no. 2, pp. 1–10, Jul. 2017, doi: 10.1515/ijeeps-2016-0233.

[5] O. Alsac and B. Stott, "Optimal load flow with steady-state security," *IEEE Trans. Power App. Syst.*, vol. PAS-93, no. 3, pp. 745–751, May 1974, doi: 10.1109/TPAS.1974.293972.

[6] S. Frank, I. Steponavice, and S. Rebennack, "Optimal power flow: A bibliographic survey I," *Energy Syst.*, vol. 3, no. 3, pp. 221–258, Sep. 2012, doi: 10.1007/s12667-012-0056-y.

[7] S. S. Reddy and P. R. Bijwe, "Real time economic dispatch considering renewable energy resources," *Renew. Energy*, vol. 83, pp. 1215–1226, Nov. 2015, doi: 10.1016/j.renene.2015.06.011.

[8] Y. Tang, K. Dvijotham, and S. Low, "Real-time optimal power flow," *IEEE Trans. Smart Grid*, vol. 8, no. 6, pp. 2963–2973, Nov. 2017, doi: 10.1109/TSG.2017.2704922.

[9] M. Massaoudi, H. Abu-Rub, S. S. Refaat, I. Chihi, and F. S. Oueslati, "Deep learning in smart grid technology: A review of recent advancements and future prospects," *IEEE Access*, vol. 9, pp. 54558–54578, 2021, doi: 10.1109/ACCESS.2021.3071269.

[10] I. Goodfellow, *Deep Learning*. Cambridge, MA, USA: MIT Press, 2016.

[11] A. Zamzam and K. Baker, "Learning optimal solutions for extremely fast AC optimal power flow," 2019, *arXiv:1910.01213*.

[12] Y. Sun, "Local feature sufficiency exploration for predicting security-constrained generation dispatch in multi-area power systems," in *Proc. 17th IEEE Int. Conf. Mach. Learn. Appl. (ICMLA)*, Cancun, Mexico, Jun. 2018, pp. 1283–1289.

[13] T. Navidi, S. Bhooshan, and A. Garg, "Predicting solutions to the optimal power flow problem," Stanford Univ., Stanford, CA, USA, Project Rep., 2016. [Online]. Available: http://cs229.stanford.edu/proj2016/report/NavidiBhooshanGarg-PredictingSolutionstotheOptimalPowerFlowProblem-report.pdf

[14] J. S. Giraldo, M. Salazar, P. P. Vergara, G. Tsaousoglou, J. G. Slootweg, and N. G. Paterakis, "Optimal operation of community energy storage using stochastic gradient boosting trees," in *Proc. IEEE Madrid PowerTech*, Madrid, Spain, Jun. 2021, pp. 1–6.

[15] X. Pan, T. Zhao, M. Chen, and S. Zhang, "DeepOPF: A deep neural network approach for security-constrained DC optimal power flow," 2019, *arXiv:1910.14448*.

[16] J. Rahman, C. Feng, and J. Zhang, "Machine learning-aided security constrained optimal power flow," in *Proc. IEEE Power Energy Soc. Gen. Meeting (PESGM)*, Denver, CO, USA, Aug. 2020, pp. 1–5.

[17] F. Diehl, "Warm-starting AC optimal power flow with graph neural networks," in *Proc. 33rd Conf. Neural Inf. Process. Syst. (NeurIPS)*, Vancouver, CA, USA, Jun. 2019, pp. 1–15.

[18] D. Owerko, F. Gama, and A. Ribeiro, "Optimal power flow using graph neural networks," in *Proc. IEEE Int. Conf. Acoust., Speech Signal Process. (ICASSP)*, Barcelona, Spain, May 2020, pp. 5930–5934.

[19] K. Baker, "Learning warm-start points for AC optimal power flow," in *Proc. IEEE 29th Int. Workshop Mach. Learn. Signal Process. (MLSP)*, Pittsburgh, PA, USA, Oct. 2019, pp. 1–6.

[20] Y. Zhou, B. Zhang, C. Xu, T. Lan, R. Diao, D. Shi, Z. Wang, and W.-J. Lee, "A data-driven method for fast AC optimal power flow solutions via deep reinforcement learning," *J. Modern Power Syst. Clean Energy*, vol. 8, no. 6, pp. 1128–1139, 2020, doi: 10.35833/MPCE.2020.000522.

[21] Y. Zhou, W.-J. Lee, R. Diao, and D. Shi, "Deep reinforcement learning based real-time AC optimal power flow considering uncertainties," *J. Modern Power Syst. Clean Energy*, early access, pp. 1–11, Sep. 2021, doi: 10.35833/MPCE.2020.000885.

[22] Z. Wang, J.-H. Menke, F. Schäfer, M. Braun, and A. Scheidler, "Approximating multi-purpose AC optimal power flow with reinforcement trained artificial neural network," *Energy AI*, vol. 7, Jan. 2022, Art. no. 100133, doi: 10.1016/j.egyai.2021.100133.

[23] T. Zhao, X. Pan, M. Chen, A. Venzke, and S. H. Low, "DeepOPF+: A deep neural network approach for DC optimal power flow for ensuring feasibility," in *Proc. IEEE Int. Conf. Commun., Control, Comput. Technol. Smart Grids (SmartGridComm)*, Nov. 2020, pp. 1–6.

[24] A. Venzke, G. Qu, S. Low, and S. Chatzivasileiadis, "Learning optimal power flow: Worst-case guarantees for neural networks," in *Proc. IEEE Int. Conf. Commun., Control, Comput. Technol. Smart Grids (SmartGridComm)*, Singapore, Nov. 2020, pp. 1–7.

[25] N. Guha, Z. Wang, M. Wytock, and A. Majumdar, "Machine learning for AC optimal power flow," 2019, *arXiv:1910.08842*.

[26] R. Canyasse, G. Dalal, and S. Mannor, "Supervised learning for optimal power flow as a real-time proxy," in *Proc. IEEE Power Energy Soc. Innov. Smart Grid Technol. Conf. (ISGT)*, New Orleans, LA, USA, Apr. 2017, pp. 1–5.

[27] F. Hasan, A. Kargarian, and A. Mohammadi, "A survey on applications of machine learning for optimal power flow," in *Proc. IEEE Texas Power Energy Conf. (TPEC)*, College Station, TX, USA, Feb. 2020, pp. 1–6.

[28] R. D. Zimmerman and C. E. Murillo-Sanchez. (2020). *MATPOWER (Version 7.1)*. [Online]. Available: https://matpower.org

[29] M. A. Pai. (1989). *IEEE 39-Bus System*. [Online]. Available: https://icseg.iti.illinois.edu/ieee-39-bus-system/

[30] S. Babaeinejadsarookolaee, "The power grid library for benchmarking AC optimal power flow algorithms," 2019, *arXiv:1908.02788*.

[31] J. J. Moré, "The levenberg–marquardt algorithm: Implementation and theory," in *Numerical Analysis*. Berlin, Germany: Springer, 1978, pp. 105–116, doi: 10.1007/BFb0067700.

[32] S. Ruder, "An overview of gradient descent optimization algorithms," 2016, *arXiv:1609.04747*.

[33] N. Qian, "On the momentum term in gradient descent learning algorithms," *Neural Netw.*, vol. 12, no. 1, pp. 145–151, 1999, doi: 10.1016/s0893-6080(98)00116-6.

[34] M. D. McKay, R. J. Beckman, and W. J. Conover, "A comparison of three methods for selecting values of input variables in the analysis of output from a computer code," *Technometrics*, vol. 42, no. 1, pp. 55–61, 2000, doi: 10.1080/00401706.2000.10485979.

[35] M. Ahsanullah, B. M. Kibria, and M. Shakil, "Normal distribution," in *Normal and Student's T Distributions and Their Applications*. Berlin, Germany: Springer, 2014, pp. 7–50.

[36] H. Rinne, *The Weibull Distribution: A Handbook*. Boca Raton, FL, USA: Chapman-Hall, 2008.

[37] Mathworks. (2021). *MATLAB, Statistics and Machine Learning Toolbox*. [Online]. Available: https://www.mathworks.com/

REHMAN ZAFAR (Student Member, IEEE) received the B.S. degree in electrical engineering from Comsats University, Islamabad, Pakistan, in 2015. He is currently pursuing the Ph.D. degree in electronics engineering with Kookmin University, Seoul, South Korea.

He has been a Graduate Researcher at Kookmin University, since 2017. His research interests include AI for power-system applications, renewable integration to power grids, and power-system control and operation.
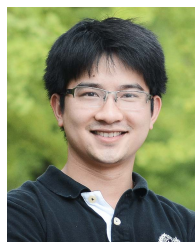
BA HAU VU received the B.S. degree in electrical and electronics engineering from the Hanoi University of Science and Technology, Hanoi, Vietnam, in 2015, and the Ph.D. degree in electronics engineering from Kookmin University, Seoul, South Korea, in 2021.

He is currently a Postdoctoral Researcher with Kookmin University. His research interests include the optimal design and operation of microgrids for high renewable-energy penetration.

IL-YOP CHUNG (Member, IEEE) received the B.S., M.S., and Ph.D. degrees in electrical engineering from Seoul National University, Seoul, South Korea, in 1999, 2001, and 2005, respectively.

He was a Postdoctoral Associate at Virginia Tech, Blacksburg, VA, USA, from 2005 to 2007. From 2007 to 2010, he worked for the Center for Advanced Power Systems, Florida State University, Tallahassee, FL, USA, as an Assistant Scholar Scientist. He is currently a Full Professor with the School of Electrical Engineering, Kookmin University, Seoul. He has carried out over 30 research projects on smart-grid technologies as the Principal Investigator and participated in various standardization works in South Korea, since 2010. His research interests include power-system control and operation, renewable-energy integration to power grids, remote microgrids with renewable energy, and shipboard power systems.

• • •